



Platinum nanocrystals supported on CoAl mixed metal oxide nanosheets derived from layered double hydroxides as catalysts for selective hydrogenation of cinnamaldehyde



Zhengbin Tian, Qingyang Li, Juying Hou, Lei Pei, Yan Li*, Shiyun Ai*

College of Chemistry and Material Science, Shandong Agricultural University, Taian, Shandong 271018, People's Republic of China

ARTICLE INFO

Article history:

Received 25 June 2015

Revised 18 August 2015

Accepted 19 August 2015

Keywords:

Cinnamaldehyde

Selective hydrogenation

Sheetlike MMO

Positively charged center

ABSTRACT

Pt nanoparticles supported on sheetlike mixed metal oxides (MMO) derived from layered double hydroxides are found to be highly efficient catalysts for the selective hydrogenation of cinnamaldehyde. A series of characterizations are employed to investigate the structure and composition of the support and catalyst. Divalent species have a significant influence on the activity and selectivity. CoAl MMO-supported catalysts achieve an increase in both conversion and selectivity to cinnamyl alcohol through the formation of PtCo alloy on the surfaces of catalysts during preparation. A possible reaction path is proposed. The effects of Co/Al ratio and calcination temperature on catalytic performance are researched in this work.

© 2015 Elsevier Inc. All rights reserved.

1. Introduction

Selective hydrogenation of α,β -unsaturated aldehydes at the carbonyl (C=O) and olefinic (C=C) groups is highly desirable in the fine chemical industry, because most of their products are important intermediates for the synthesis of many chemicals [1]. Cinnamaldehyde (CAL) is a particularly important α,β -unsaturated aldehyde, since its partial hydrogenation products are important intermediates in the manufacture of chemicals (particularly perfumes, flavors, and pharmaceuticals) [2,3]. Also, it is considered a good model for investigating the catalytic behavior of the microstructures of heterogeneous catalysts. The selective hydrogenation of CAL is a rather complex reaction network involving several important intermediates and a number of series-parallel reactions. Two main competitive products of selective hydrogenation, hydrocinnamaldehyde (HCAL) and cinnamyl alcohol (COL), can be produced through the hydrogenation of the conjugated C=C or C=O bond over the supported metal catalysts (Scheme 1). Further hydrogenation of these two intermediates results in the formation of hydrocinnamyl alcohol (HCOL).

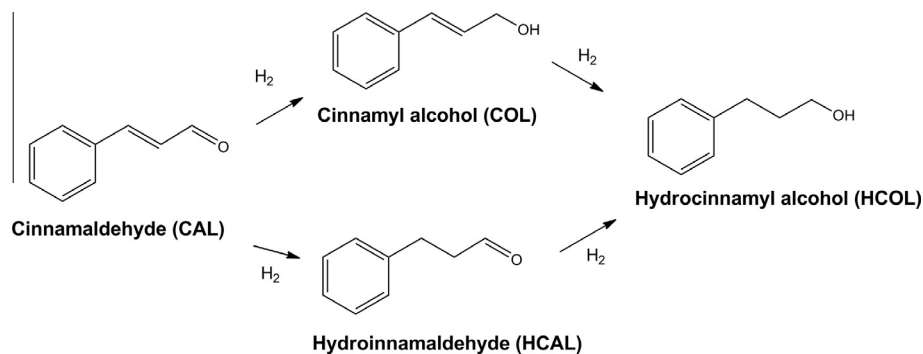
However, the development of catalysts for the selective hydrogenation of CAL to COL is still challenging. Because the C=O bond presents a higher binding energy than the C=C bond (715 kJ/mol and 615 kJ/mol, respectively) [4], the reduction of the C=C bond is thermodynamically more favorable than that of C=O bond. In

the catalytic process, the undesirable product HCOL would largely be formed, decreasing the selectivity to the unsaturated alcohol. Over the past few years, common noble metal (Pd, Pt, Ru, and Au)-based catalysts have been used for the hydrogenation of CAL [5–7]. Unfortunately, only a few catalysts are suitable for the purpose of C=O hydrogenation; most of these are Pt-based catalysts. Hence, maintaining high selectivity of Pt-based catalysts while increasing their activity has become an urgent task for further development in this field. Many studies have been devoted to enhancing the selectivity of catalysts toward the unsaturated alcohol either by fine control of the sizes [8] and/or the exposed facets of the active metal nanoparticles [9], by exploiting the steric constraints imposed by the environment of the active site [10], by decorating the primary metal with a second metal component [11], or by adding promoters such as an alkali element [12].

It is well known that there is an interaction between the support and active metal sites that can modify the catalytic properties of the metal catalyst. This is a feasible way to search for appropriate materials used as catalyst supports for preparing highly active and selective catalysts for the hydrogenation of CAL. Traditional carbon materials, such as activated carbon, carbon aerogel [13], and CNTs [14], and SiO₂ [8,15] have been widely used as catalyst supports. However, there is little metal-support interaction effect among the catalysts because of the almost electroneutral surface of the support, resulting in low conversion and poor selectivity. The efficient supports presenting a strong metal-support interaction effect (SMSI effect), such as TiO₂, favor the activation of the carbonyl group. That is because there is a strong interaction

* Corresponding authors. Fax: +86 538 8247660.

E-mail addresses: liyan2010@sdau.edu.cn (Y. Li), ashy@sdau.edu.cn (S. Ai).



Scheme 1. The reaction pathway and main products for hydrogenation of CAL.

between the carbonyl group and the positively charged center ($\text{TiO}_x^{\delta+}$) [16]. However, we found that a large amount of HCOL was produced when TiO_2 -supported Pt particles were used in the previous studies. The same phenomenon was observed in high-valent Al_2O_3 -supported Pt particles. To improve the selectivity to COL, the structure modification of this support is presented.

Layered double hydroxides (LDH) are a class of synthetic highly ordered two-dimensional anionic clays consisting of positively charged layers (two metallic ions) with charge-balancing anions, which are octahedrally coordinated in the sheets [17,18]. They can be expressed by the general formula $[\text{M}_{1-x}^{2+}\text{M}_x^{3+}(\text{OH})_2](\text{A}^{n-})_{x/n} \cdot m\text{H}_2\text{O}$, where A^{n-} is a nonframework charge-compensating anion (CO_3^{2-} , SO_4^{2-}). M^{2+} and M^{3+} are divalent (Mg^{2+} , Zn^{2+} , Ni^{2+} , Co^{2+}) and trivalent cations (Al^{3+} , Fe^{3+}), respectively [19,20]. Mixed metal oxides (MMO) can be generated from LDH by thermal treatment (450–600 °C), by which MMO not only inherits structural features of LDH, but possess high specific surface area, thermal stability, and tunable surface acidic/basic properties [21,22]. Based on these properties, they can be widely employed as promising heterogeneous catalysts and supports. This inspired us to fabricate a MMO-supported Pt catalyst for the selective hydrogenation of CAL. The resulting Pt-based catalyst may possess the following advantages: (i) the MMO matrix would provide a confined and stable microenvironment to disperse metal particles uniformly; (ii) thermal stability and mechanical stability of the structured architecture can significantly improve the stability of the catalyst and facilitate its regeneration; (iii) inherent Lewis basic sites promote the selectivity of the C=O bond without the need of a foreign alkali; (iv) mutual substitution of divalent and trivalent cations not only generates the SMSI effect at the interface, which would facilitate the activity of the catalyst, but also promotes the selectivity of the C=O bond.

In this report, we prepared eight hydrogenation catalysts by supporting Pt nanoparticles on a series of Al-based MMO (divalent metal: Co, Ni, Zn, Mg) and corresponding LDH precursors. The performance of different catalysts was investigated and compared in the selective hydrogenation of CAL to COL under mild reaction conditions. We found that divalent species have a significant influence on activity and selectivity, and high activity and selectivity was obtained on the CoAl-MMO supported catalyst. A series of characterizations were employed to investigate the structure and composition of the Pt/CoAl-MMO and the characterizations of the Pt/CoAl-LDH, Pt/ZnAl-LDH, and Pt/CoAl-MMO are provided for comparison. The surface properties of CoAl-MMO, such as Lewis basic sites, depend on the composition and pretreatment parameters, such as Co/Al ratio and activation temperature. These effects were also researched in this work.

2. Experimental

2.1. Materials

Hexachloroplatinic acid ($\text{H}_2\text{PtCl}_6 \cdot 6\text{H}_2\text{O}$, 99.9%) was purchased from Aldrich Co. Ltd. Cinnamaldehyde (98%) was purchased from Aike Chemical Reagent Co. Ltd (Chengdu, China). Other chemicals were analytical grade and not further purified prior to use. Distilled deionized water was utilized through the experiments. The purity of hydrogen was 99.9%.

2.2. Catalyst preparation

NAI-MMO (N = Co, Ni, Mg, Zn) support was derived from an NAI-LDH precursor. The NAI-LDH LDH precursor was synthesized using the homogeneous precipitation method. A mixed solution

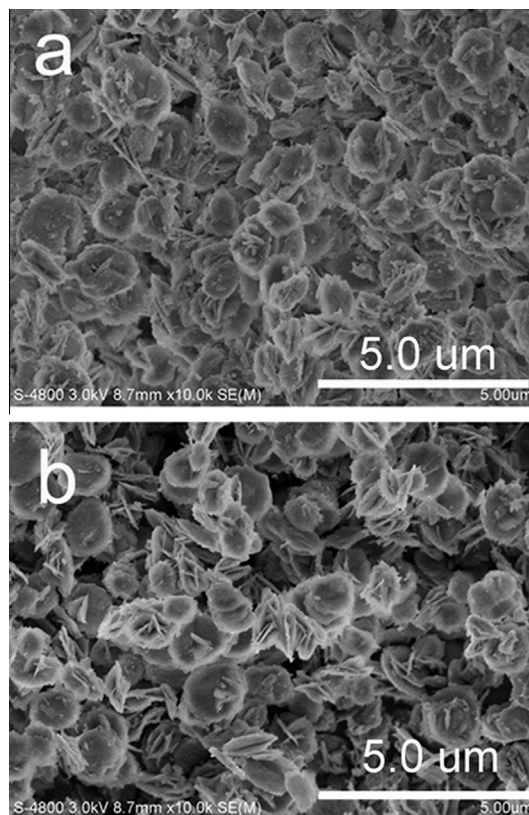


Fig. 1. SEM images of (a) CoAl-LDH and (b) CoAl-MMO.

of 0.1 M NiCl_2 and 0.05 M AlCl_3 ($R = 0.66$, $\text{Co}/(\text{Co} + \text{Al})$ mole ratio) and 0.5 M urea was transferred to an autoclave and hydrothermally treated at 110°C for 12 h. The precipitate was filtered, washed, dried at 60°C under vacuum, and transformed into NiAl-MMO support after calcination at 450°C for 4 h.

The Pt catalyst was prepared using a reduction–deposition method. The support was impregnated in an aqueous solution of H_2PtCl_6 at 80°C for 5 h in a round-bottom flask. Then 20 mL of 0.1 mol/L NaBH_4 solution was added dropwise to the flask under vigorous stirring for another 1 h. Afterward, the slurry was filtered and the solid was washed with water until the filtrate was neutral. The solid obtained was dried at 45°C under vacuum for 12 h before use. The nominal content of Pt in the catalyst was 2 wt.%. $\text{PtCo}/\text{ZnAl-MMO}$ and $\text{PtNi}/\text{ZnAl-MMO}$ were prepared by the same method, adding $\text{Co}(\text{NO}_3)_2$ and $\text{Ni}(\text{NO}_3)_2$ as metal precursors, respectively.

2.3. Materials characterization

X-ray diffraction (XRD) patterns were measured at room temperature using a Bruker D8 Advance X-ray diffractometer with $\text{Cu K}\alpha$ radiation at 40 kV and 30 mA. Thermal analysis of sample was performed using thermogravimetric analysis (TGA) on a simultaneous thermal analyzer (SDT Q600, TA, USA) from room temperature to 800°C with a heating rate of $10^\circ\text{C}/\text{min}$. The surface

functional groups in samples were measured by FT-IR using a Thermo Scientific Nicolet 380 spectrometer (USA) with a spectral range from 4000 to 400 cm^{-1} at a spectral resolution of 4 cm^{-1} and 32 scans. SEM analysis was carried out using a NoVaTM Nano SEM 430 scanning electron microscope (FEI, USA) at an electron acceleration voltage of 20 kV. A Multimode Nanoscope IIIa atomic force microscope (Veeco, USA) was used in tapping mode. Transmission electron microscopy (TEM) was carried out with an FEI Tecnai G20 (USA) with an accelerating voltage of 200 kV. The textural properties of samples were determined by nitrogen sorption isotherms on a Micromeritics ASAP 3020 instrument (USA) at 77 K. The surface area and pore volume were calculated using BET and BJH methods, respectively. XPS was measured with a K-Alpha XPS system (Thermo Fisher Scientific, USA) using monochromatic $\text{Al K}\alpha$ as the excitation source (1486.6 eV).

2.4. Hydrogenation reaction

The hydrogenation reactions were carried out in a stainless autoclave reactor with a 50 mL Teflon sleeve. In a typical procedure, 0.1 g catalyst was dispersed in 19 mL ethanol and then 8.2 mmol CAL was added into the solution. The reactor was sealed, purged three times with H_2 , and then pressurized to 2.0 MPa. The reaction was conducted at 70°C with a stirring speed of 750 rpm for 2 h. The reaction mixture was analyzed by a Shimadzu

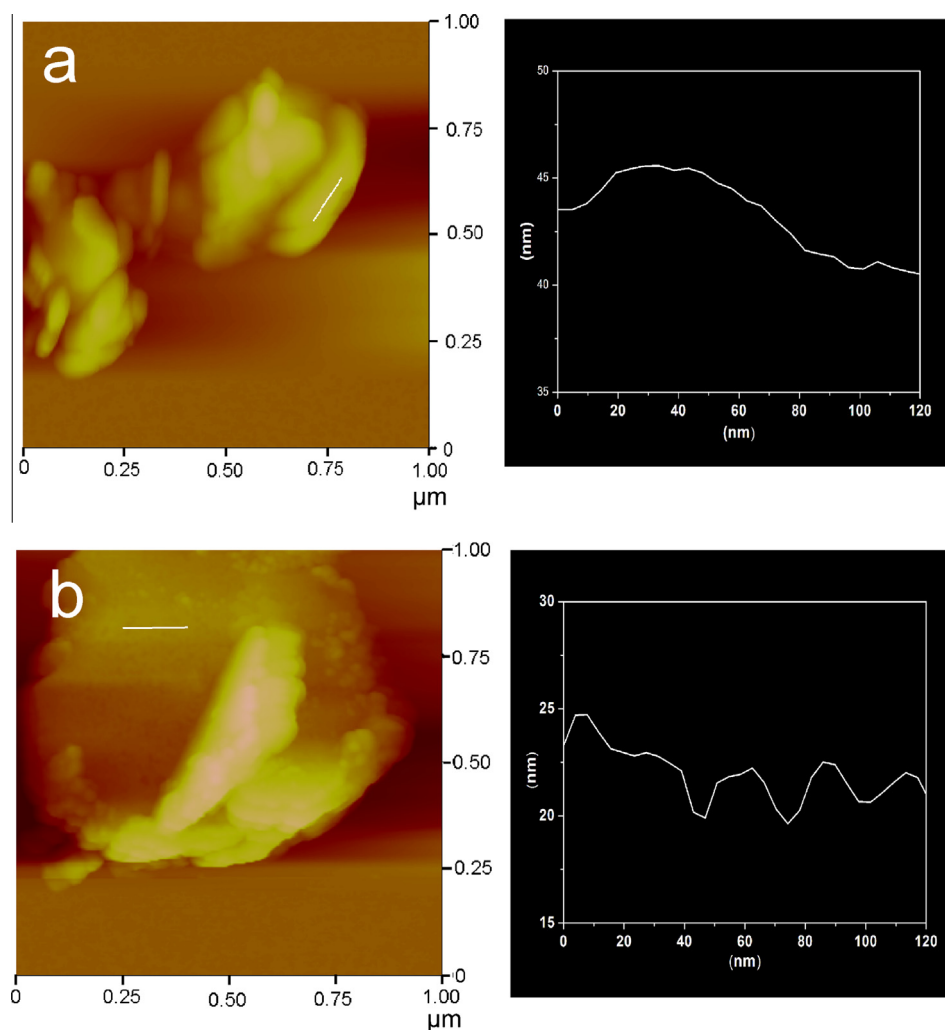


Fig. 2. AFM images of CoAl-LDH and CoAl-MMO.

GC-2010 gas chromatograph with a flame ionization detector (FID) system.

3. Results and discussion

3.1. Support and catalyst characterization

CoAl-LDH was synthesized using a conventional coprecipitation method by the urea slow hydrolysis process. The CoAl-LDH product was a very fine pink powder and could be well dispersed in water. The SEM image in Fig. 1a shows relatively uniform nearly circular sheet-like microcrystals with diameter 1.0–1.5 μm and thickness 100–200 nm. The magnification SEM image reveals the existence of a hierarchical structure that is composed of randomly oriented two-dimensional LDH sheets affording a rough surface. Calcination of the LDH sheets leads to their transformation to MMO sheets. As shown in Fig. 1b, the MMO inherits the original sheetlike morphology of the LDH precursor with a little shrinkage of the circular structure, indicating that there is a collapse on the surface of the obtained MMO. AFM characterization further reveals a collapse corresponding to the SEM image, as clearly shown from the height line profile in Fig. 2.

From the FTIR (Fig. 3a), a broad absorption band at around 3100–3700 cm^{-1} is attributed to the O–H stretching vibrations of the hydroxyl groups in the hydroxalate layers and interlayer water molecules. The characteristic peaks belonging to stretching and bending modes of CO_3^{2-} are observed at 1359 and 770 cm^{-1} ,

respectively, suggestive of the presence of interlayer carbonate anions. The H_2O bending vibration occurs at 1629 cm^{-1} , and other absorption bands below 800 cm^{-1} belong to metal–oxygen (M–O) and metal–hydroxyl (M–OH) vibrations in the lattice of the hydroxalate. After CoAl– CO_3^{2-} -LDH is calcined at 450 $^\circ\text{C}$, the sharp absorption peak at 1359 cm^{-1} and the broad peak at 770 cm^{-1} representing CO_3^{2-} completely disappear. For the obtained CoAl-MMO, two obviously sharp peaks at 662 cm^{-1} and 562 cm^{-1} are attributed to the enhanced M–O vibrations. This implies that CoAl-LDHs have transformed into CoAl-MMO with the absence of CO_3^{2-} and the attendance of large numbers of M–O bonds.

Fig. 3b shows the TG–DTA curves of CoAl-LDH, which can be divided into three stages. The initial one between 40 and 125 $^\circ\text{C}$ is mainly due to water release from the surface and the interlayer. The second weight loss stage corresponds to 125–225 $^\circ\text{C}$ and can be assigned to removal of interlayer water molecules and CO_2 (from intercalated CO_3^{2-}). The third stage, with maximum mass loss at 262 $^\circ\text{C}$, can be attributed mainly to the thermal decomposition of brucite-like layers through the removal of OH groups as water molecules. The process of thermal decomposition is shown by the FTIR spectra of LDHs calcined at different temperatures (Fig. S2). The spectra demonstrate the vanishing of CO_3^{2-} stretching modes at 200 $^\circ\text{C}$ and the increase of intensity of O–M vibrations attributed to metal oxides with increasing annealing temperature.

Fig. 3c shows the powder XRD patterns of as-prepared product; peaks characteristic of an LDH structure were clearly observed in

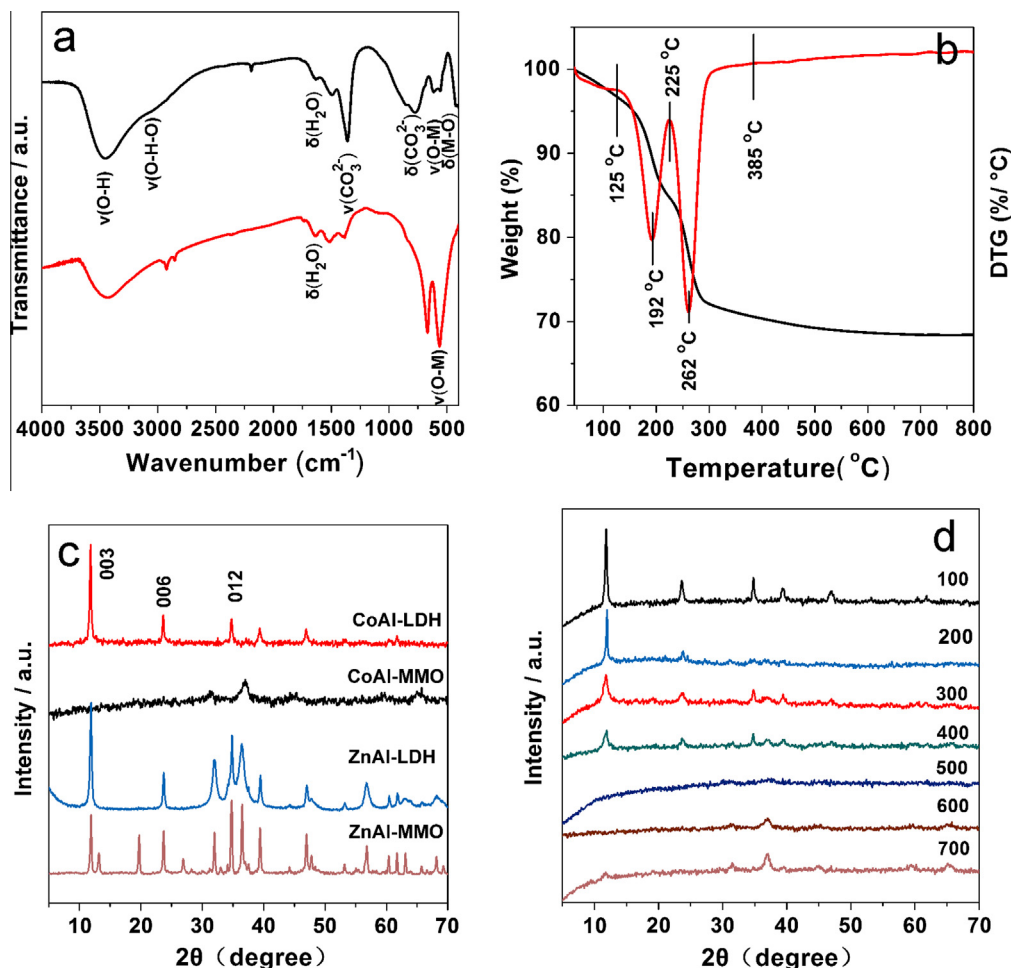


Fig. 3. (a) FTIR of CoAl-LDH and CoAl-MMO; (b) DTA–TG curves for CoAl-LDH; (c) XRD patterns of CoAl-LDH, CoAl-MMO, ZnAl-LDH, and ZnAl-MMO; (d) XRD patterns for CoAl-MMO obtained at different temperatures.

the CoAl-LDH. The two basal reflections of (003) and (006) with d values of 0.748 and 0.375 nm, respectively, can be indexed as a rhombohedral structure with refined lattice parameters of $a = 0.3064$ and $c = 2.2573$ nm, which are consistent with those of well-known LDH materials in CO_3^{2-} form [23]. No peaks of impurities were discerned, implying the high crystallinity and fine purity of the LDH. This shows that the CoAl-LDH and corresponding MMO are uniform. As shown in Fig. 3c, as-prepared CoAl-MMO exhibit XRD patterns consistent with an amorphous structure, which is significantly different from the high crystallinity of ZnAl-MMO. The annealing experiments of CoAl-LDH from 100 to 700 °C shows that conversion from rhombohedral to amorphous structure, in which a weak peak at 37.0° is observed and attributed to the (3 1 1) reflection of CoAl_2O_4 [24].

Specific surface area and pore size determination of LDH and corresponding MMO are critically important, since their surface properties dominate the interfacial behavior when they are used as support, and the porosity and surface area of the different catalysts were characterized by N_2 sorption measurements. Fig. 4 shows the N_2 adsorption–desorption isotherms and BJH pore size distribution curves for Pt/AlCo-LDH, Pt/AlCo-MMO, Pt/AlZn-LDH, and Pt/AlZn-MMO, respectively, and corresponding data are summarized in Table 1. All the samples exhibit mixed isotherms of type II (at high p/p_0) and type IV adsorption (at lower p/p_0) with an H3-type hysteresis loop in the region of relative pressure 0.4–1.0, which is associated with capillary condensation taking place in mesopores. The Type H3 loop without any limiting adsorption at high p/p_0 is observed with aggregates of platelike particles giving rise to slit-shaped pores, which is also identical to the SEM images [25,26]. The abrupt closure of the hysteresis loop at ca. $p/p_0 = 0.43$ indicates the presence of mesopores <4 nm. The pore size distribution derived from the adsorption branch further clearly shows that all the samples have mesopores with a narrow size distribution centered in the range 3–4 nm. From Table 1, it is very interesting

to note that BET surface area, pore volume, and pore diameter increased after calcination. The magnitude of these values for LDH depends on the nature of the structure, such as homogeneous morphology, and the original stacking. The increase for MMO may be attributed to explosion of CO_2 released from decomposition of intercalated CO_3^{2-} at high temperature. Additionally, these values of Zn species are slightly higher than those of Co species, while Zn-species-supported catalysts show poor activity for the selective hydrogenation of COL. The result indicates that the specific surface area, pore volume, and pore diameter of the catalyst are not dominant factors in determining its activity. It is the effective exposure of active sites that is more crucial.

TEM also shows the sheetlike structure of Co species support and the shrinking of circular structure after calcination, while ZnAl-LDH and -MMO are composed of sheetlike and clubbed structures together (Fig. S5). The Pt catalyst was prepared using the conventional impregnation–reduction–deposition method with NaBH_4 as reductant. The representative TEM images of the supported Pt catalysts are obtained to visually confirm the distribution size of Pt NPs. The images (Fig. 5) show that monodisperse Pt nanoparticles are uniformly decorated on different supports with different average sizes, and no significant formation of aggregates is observed. Pt nanoparticles supported on Co species

Table 1
Comparison of some parameters of the different supported Pt catalysts.

Catalyst	BET surface area (m^2/g)	BJH surface area (m^2/g)	Pore volume (cm^3/g)	Pore diameter (nm)
Pt/AlCo-LDHs	55.06	55.12	0.165	3.22
Pt/AlCo-MMO	87.14	123.3	0.289	3.83
Pt/AlZn-LDHs	65.88	45.79	0.142	3.14
Pt/AlZn-MMO	98.70	110.4	1.255	3.83

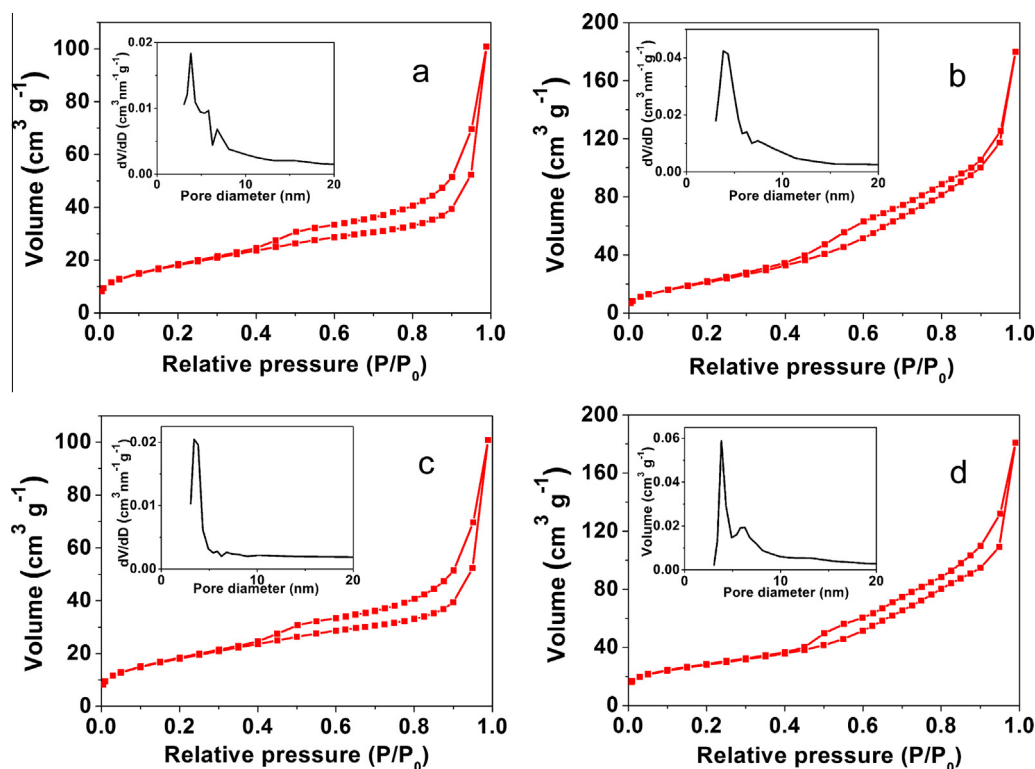


Fig. 4. Nitrogen adsorption–desorption isotherms and corresponding pore size distribution curves (inset) of (a) Pt/CoAl-LDH, (b) Pt/CoAl-MMO, (c) Pt/ZnAl-LDH, and (d) Pt/ZnAl-MMO.

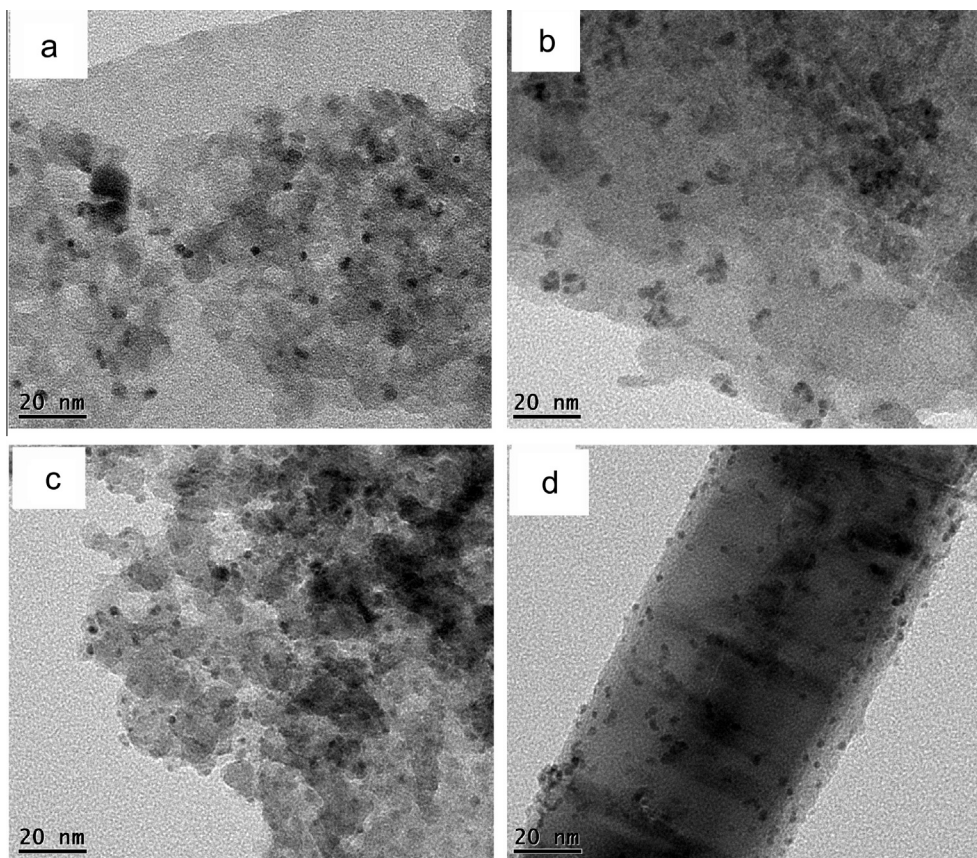


Fig. 5. TEM images of (a) Pt/CoAl-LDH, (b) Pt/CoAl-MMO, (c) Pt/ZnAl-LDH, and (d) Pt/ZnAl-MMO.

support, especially for CoAl-MMO, present a larger size of 4–5 nm. For the Zn-species-supported Pt catalysts, it is found that the Zn species promotes the dispersion of the metals on the support surface, which results in a quite uniform particle size distribution of 2–3 nm. However, it was found that large metal particles (>3 nm) favor high selectivity for COL [27]. Moreover, there is a visible difference in the morphology of metal nanoparticles. Most of the Pt nanoparticles are pseudo-spherical in shape, while Pt nanoparticles supported on CoAl-MMO present an irregular shape.

To analyze the elemental composition as well as the chemical bonding environment of Co and added Pt, XPS measurements were conducted on CoAl-MMO and Pt/CoAl-MMO. Both survey spectra (Fig. 6a) show the Co2p peak at 780 eV, O1s at 530 eV, and Al2p at 74 eV, respectively, and no other elements such as chlorine and sodium are observed. C1s peaks are displayed in the survey spectrum, indicating the residue of carbon element. Although overlapped with the Al2p peak, the Pt4f peak is distinguished with ease (Fig. 6b). The Pt4f region shows two doublets from the spin-orbital splitting of the $4f_{7/2}$ and $4f_{5/2}$ states, respectively peaked at 71.5 ± 0.1 eV and 75.0 ± 0.1 eV with integral peak area close to a value of 4:3, which is mainly assigned to zerovalent Pt⁰ in the metallic state [18]. The Co2p spectrum (Fig. 6c) shows the presence of the $2p_{3/2}$ and $2p_{1/2}$ states. The main Co $2p_{3/2}$ peaks for the two samples were found to be at 780.4 eV, which reveals that Co is mainly in the oxidized state. In the case of Pt/CoAl-MMO, a minor contribution was recorded at a lower binding energy of 778.2 eV and 793.5 eV leading to a shoulder attributed to metallic Co in the Co $2p_{3/2}$ and Co $2p_{1/2}$ region, indicating the Co²⁺ was partly reduced during the preparation of the catalyst. Metallic Ni is observed as well in the Ni2p region in Pt/NiAl-MMO (Fig. S6) and metallic Zn is not observed as expected in Pt/ZnAl-MMO (Fig. S7). Elemental mapping by HAADF-STEM reveals the

uniformity of Pt/CoAl-MMO catalyst. Pt atoms are homogeneously distributed throughout the uniform CoAl-MMO framework, as illustrated in Fig. 7.

3.2. Hydrogenation of CAL over the Pt catalysts

Some properties of the catalysts, such as the sorts of transition metal, particle size, types of support, and preparation method, might dominate the selective hydrogenation of CAL. Here, the various LDH- and derived MMO-supported Pt nanoparticles were tested in the hydrogenation reaction of CAL under the same mild conditions for the investigation of the support effect, which was carried out in a stainless steel autoclave. It can be seen from Table 2 divalent species have a significant influence on activity and selectivity. Among them, transition metal species, cobalt and nickel, and LDH- and MMO-supported catalysts exhibit higher activity than the other catalysts. The hydrogenation over Pt/CoAl-MMO and Pt/CoAl-LDH catalysts affords COL with 75.9 and 74.2% selectivity with a reaction conversion of 93.1 and 94.3%, respectively. They present higher conversion and selectivity than that obtained over conventional Pt/CNTs (conversion 87.2% and selectivity 48.3%) [14] and higher conversion than that catalyzed on Pt/SBA-15 (conversion 16%) [15]. Though Pt/NiAl-MMO and Pt/NiAl-LDH achieve high conversion, poor selectivity is obtained simultaneously. Transition metals have been employed widely as co-catalysts in a wide variety of hydrogenation reactions. Pristine LDH and MMO show no catalytic activity for this hydrogenation reaction. When the supports were treated with sodium borohydride solution in the absence of Pt precursor, Co-based and Ni-based LDH and MMO supports exhibited little catalytic activity, owing to the presence of Co and Ni in the metallic state, which has been shown in the XPS Co2p and Ni2p spectra. This shows that

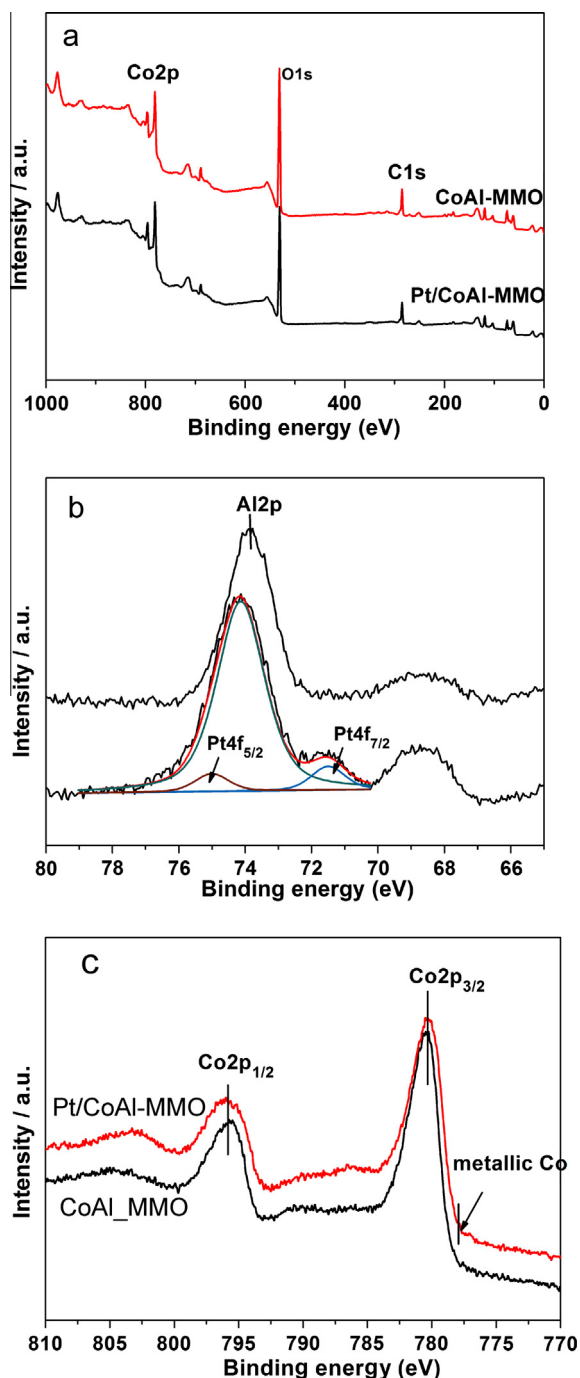


Fig. 6. XPS spectra of the CoAl-MMO and Pt/CoAl-MMO samples: (a) survey spectrum; (b) Al2p and Pt4f spectra; and (c) Co2p spectrum.

single metallic Co and Ni have little catalytic activity in the hydrogenation reaction. However, PtCo/ZnAl-MMO and PtNi/ZnAl-MMO catalysts present a result similar to Pt/CoAl-MMO and Pt/NiAl-MMO, indicating there must be an interaction between Pt nanoparticles and transition metals. Most likely, the Co^{2+} and Ni^{2+} were partly reduced and formed PtCo and PtNi alloy on the surface of the catalyst during the preparation.

A possible reaction mechanism over the Pt/CoAl-MMO catalyst was proposed (Scheme 2), illustrating that the hydrogenation of CAL proceeds through cooperation between the bimetallic PtCo alloy and the Al^{3+} sites on the surface of the CoAl-MMO support. Generally, CAL can absorb onto the surfaces of catalysts via two

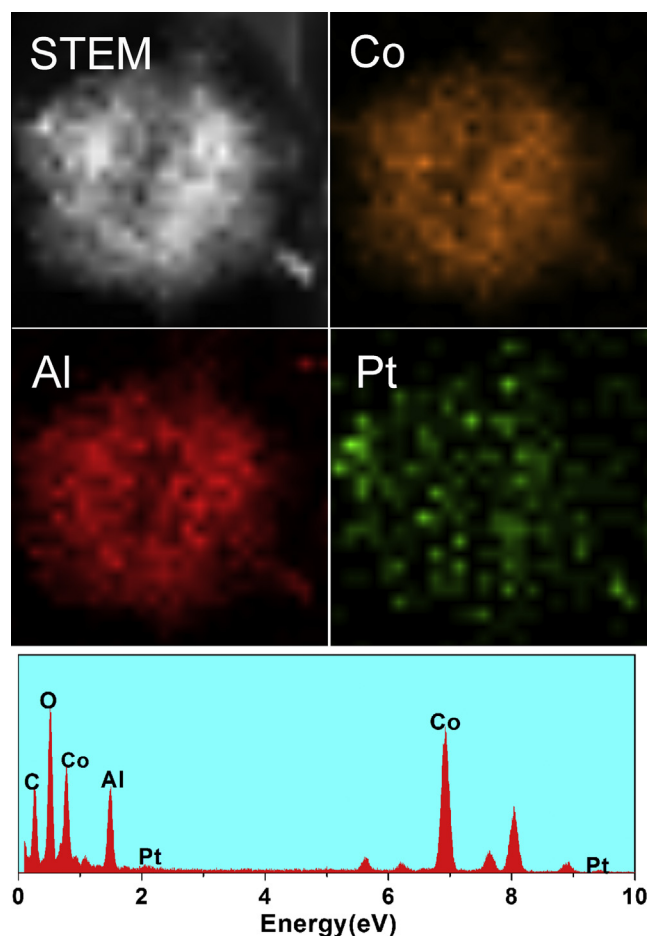


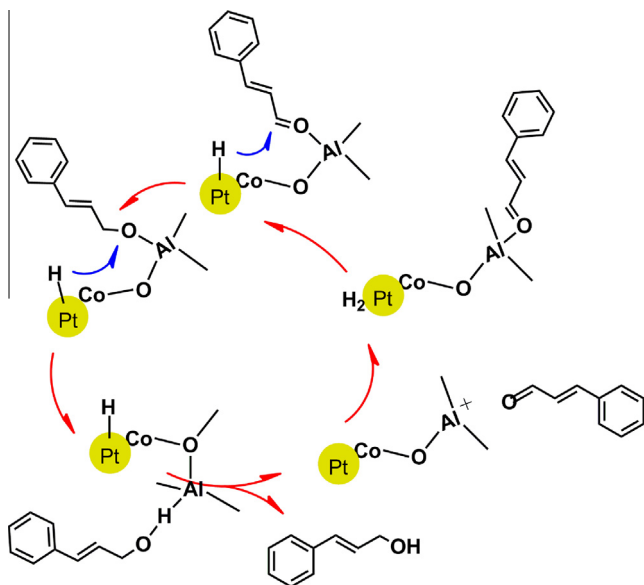
Fig. 7. HAADF-STEM and STEM-EDX elemental mapping images of Pt/CoAl-MMO.

Table 2
The effect of support on catalytic performance.

Catalyst	Conversion (%)	Selectivity (%)		
		HCAL	HCOL	COL
Pt/CoAl-MMO	93.1	11.8	12.3	75.9
Pt/CoAl-LDH	94.3	14.3	11.5	74.2
Pt/NiAl-MMO	97.5	38.6	55.5	5.9
Pt/NiAl-LDH	85.8	38.1	28.9	33.0
Pt/MgAl-MMO	20.4	66.5	7.4	26.1
Pt/MgAl-LDH	73.8	23.6	12.3	64.1
Pt/ZnAl-MMO	15.4	50.4	17.5	32.3
Pt/ZnAl-LDH	10.1	39.5	18.1	42.4

Note: Reaction conditions: 8.2 mmol CAL, 19.0 mL $\text{C}_2\text{H}_5\text{OH}$, 70 °C, 2.0 MPa, 2 h.

competing mechanisms, a vertical $\text{C}=\text{O}$ atop geometry and a planar geometry through the $\text{C}=\text{C}$ double bond, which give two products, COL and HCAL, respectively. In this mechanism, the CAL is absorbed via the vertical $\text{C}=\text{O}$ atop geometry though the interaction between the carbonyl group and positively charged center Al^{3+} and the carbonyl group is activated. In the second step, the activated H atom attacks the C atom in the carbonyl group. It is speculated that this step may determine the conversion and the selectivity, which are related to the metal species. The following step of the activated H atom attacking the O atom proceeds quickly and the catalytic cycle is completed. The COL does not further convert to the fully saturated form HCOL, whereas the HCAL easily converts to HCOL though the path shown in the proposed mechanism.



Scheme 2. The possible reaction pathway of hydrogenation of CAL over Pt/CoAl-MMO catalyst.

Pt/CoAl-MMO and Pt/CoAl-LDH exhibit similar catalytic activity; however, CoAl-LDH has less thermal stability and is hard to regenerate. Therefore, Pt/CoAl-MMO is selected as the reaction catalyst in most studies. Fig. 8 presents the results for the optimal Pt/CoAl-MMO catalyst for the selective hydrogenation of CAL at various temperatures and reaction times. The CAL conversion shows an increasing trend with elevated reaction temperature, as shown in Fig. 8a. The conversion of CAL increases sharply from 21.0% to 92.2% when the temperature rises from 20 to 60 °C. The temperature also influences the selectivity: The HCAL selectivity shows a decreasing trend, while the selectivity toward HCOL presents the reverse tendency. The selectivity to COL remains almost unchanged (75%). This study thus implies that although Pt/CoAl-MMO catalyst is effective even at low temperature for the selective hydrogenation of carbonyl groups of CAL, higher temperature further facilitates the process of conversion, resulting in a high COL yield. When the temperature was elevated to 80 °C, the COL selectivity decreased slightly, while the quantity of undesired HCOL increased remarkably to 18%. It is concluded that COL is prone to transform into HCOL at high temperature. This reveals that COL is a less thermodynamically stable product, although a desired

one, and it is more difficult to achieve high selectivity to COL. Fig. 8a shows the variation of CAL conversion and product selectivity as a function of reaction time for Pt/CoAl-MMO. The reaction time sharply influenced the conversion of CAL, but it had little effect on selectivity of COL, which is similar to the temperature effect. In contrast, the selectivity of HCAL decreases and that of HCOL increases, because the HCAL was converted to HCOL by further hydrogenation of the C=O bond. These results imply that the hydrogenation of C=C and C=O bonds does not take place in parallel on the Pt/CoAl-MMO, which is consistent with Wu et al. [28].

The effect of calcination temperature of the CoAl-LDH on the CAL reaction was studied, and the results are given in Table 3. Calcination temperature greatly influences the catalytic reaction. When the MMO was obtained at 200 and 300 °C, the catalyst showed bad activity with the lowest conversion (ca. 4%) among the series. When the calcination temperature was elevated to 400 °C, the conversion of CAL sharply increased to 93.1%, while the quantity of undesired HCOL remarkably increased to 66.3%. When the temperature was further elevated to 500 °C and subsequently the calcination temperature was increased from 500 to 700 °C, the conversion of CAL remained above 95% and the selectivity to COL increased to 72% and decreased with increasing temperature.

The effect of Co/Al ratio was also researched. Fig. 9 shows the relation between Co content ($R = \text{Co}/(\text{Co} + \text{Al})$ mole ratio) and conversion and selectivity. It is found that the conversion of CAL over the Pt/CoAl-MMO catalysts decreased with a rise in the Co content from 100% ($R = 0$) to 88.9% ($R = 1$). Also, the rise of Co in the Pt/CoAl-MMO catalyst could obviously improve the selectivity of COL from 4.7% to 80.0%. When $R = 0$, the support is bare Al_2O_3 , which has a positively charged center like $\text{TiO}_x^{\delta+}$. The strong positively charged center favors the activation of the carbonyl group,

Table 3
The effect of calcination temperature of CoAl-LDH on catalytic performance.

Temperature	Conversion (%)	Selectivity (%)		
		HCAL	HCOL	COL
200	3.2	53.7	23.7	22.6
300	4.5	69.1	17.3	13.6
400	93.1	22.2	66.3	12.5
500	94.5	12.3	14.2	73.5
600	99.7	16.8	10.7	72.5
700	97.2	17.2	11.8	71.0

Note: Reaction conditions: 8.2 mmol CAL, 19.0 mL $\text{C}_2\text{H}_5\text{OH}$, $R = 0.66$, 0.1 g catalyst, 70 °C, 2.0 MPa, 2 h.

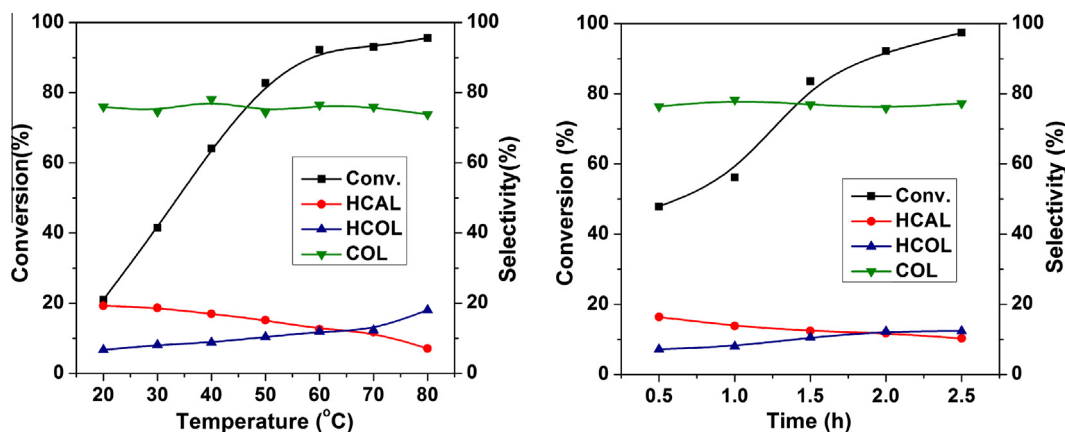


Fig. 8. Effects of temperature (a) and reaction time (b) on CAL hydrogenation performance with the Pt/CoAl-MMO catalyst (reaction conditions: (a) 0.1 g catalyst, 2.0 MPa, 2 h; (b) 0.1 g catalyst, 2.0 MPa, 70 °C).

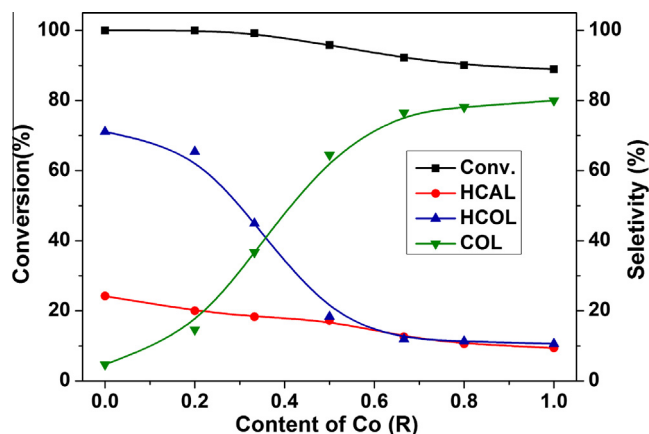


Fig. 9. The effect of Co/Al ratio (R) on CAL hydrogenation performance.

and complete conversion is obtained. However, plenty of HCOL was produced, which may be because the strong interaction between the carbonyl group and positively charged center facilitates further hydrogenation. With increasing Co content, the trivalent Al center is surrounded gradually by divalent Co atoms and the charge of the trivalent positive center is dispersed, which results in a decrease of conversion but an increase in selectivity. Meanwhile, the addition of Co also introduces active transition metal sites. When $R=0$, that is, the support is pure CoO, high selectivity is achieved, indicating that CoO is a superior support for C=O hydrogenation.

For heterogeneous systems, one important issue is to verify the stability and reusability of the catalyst during the course of reaction. A recycling experiment is performed to elucidate this point. For the Pt/CoAl-MMO catalyst (Fig. 10), it is noted that the conversion decreased slightly as the recycle times increased. Through there is a decrease, good catalytic activity (>87% conversion) is achieved after the fourth run. The formation of carbon deposits on the surface of the catalyst may partly cover active centers and result in a decrease in catalytic activity. The COL selectivity has a sharp decrease from 75% (first use) to 58% (fourth use), mostly owing to oxidation of active Pt on the catalysts. A similar phenomenon is observed in the case of Pt/CoAl-LDH catalyst (Fig. S9). Before the fifth run, the Pt/CoAl-MMO catalyst was recalculated at 450 °C and re-reduced with NaBH₄, and Pt/CoAl-LDH was merely re-reduced. For Pt/CoAl-MMO, activity and selectivity

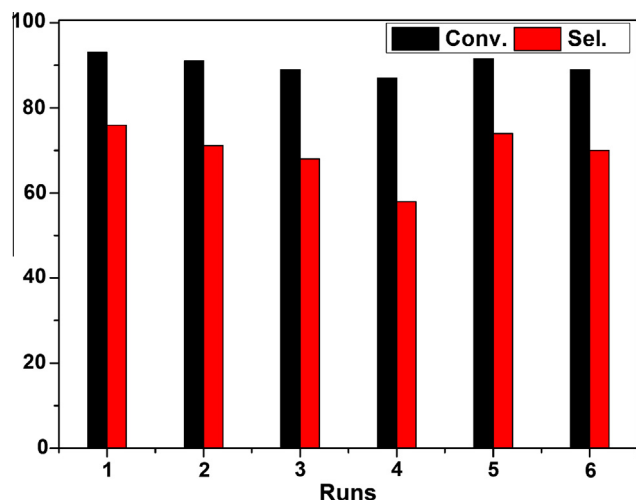


Fig. 10. Recycling use of the Pt/CoAl-MMO catalyst. Reaction conditions: 8.2 mmol CAL, 19.0 mL C₂H₅OH, 0.1 g catalyst, 70 °C, 2.0 MPa, 2 h.

toward COL consistent with the first use is regenerated, while Pt/CoAl-LDH just regains high selectivity toward COL and loses high conversion. The result reveals the formation of carbon deposits during the course of reaction and the oxidation of active Pt. The TEM images (Fig. S10) further reveal that the shape and morphology of the catalyst after six runs was not subject to serious damage during the reactions, demonstrating the high stability and reusability of the catalyst under the investigated conditions.

4. Conclusion

We have synthesized a series of Al-based LDH- and corresponding MMO-supported Pt catalysts using the conventional impregnation–reduction–deposition method with NaBH₄ as reductant, and investigated their catalytic behavior in the selective hydrogenation of CAL.

The MMO inherits the original sheetlike morphology of the LDH precursor and processes the collapse on the surface, and has increasing BET area and pore volume and high thermal stability. Divalent species have a significant influence on the activity and selectivity. CoAl-MMO supported catalysts achieve an increase in both activity and selectivity to COL due to the formation of PtCo alloy on the surface of catalysts during preparation. TEM also reveals that Pt/CoAl-MMO has large metal particles (>3 nm), which favor high selectivity for COL, and HAADF-STEM elemental mapping reveals the uniformity of Pt/CoAl-MMO catalyst. Particularly, the possible mechanism of cooperation between the bimetallic PtCo alloy and the Al³⁺ sites further facilitates the process of CAL hydrogenation. The calcination temperature influences the activity and selectivity greatly. Research on the effect of the Co/Al ratio shows that addition of Co to the support disperses the charge of the trivalent ion, resulting in a slight decrease in conversion but an obvious increase in selectivity. The Pt/CoAl-MMO catalysts can be reused for three runs without appreciable loss of activity and regenerated by calcination and reduction with NaBH₄, indicative of excellent stability.

Acknowledgment

The authors gratefully acknowledge financial support from the National Natural Science Foundation of China (No. 21203113).

Appendix A. Supplementary material

Supplementary data associated with this article can be found, in the online version, at <http://dx.doi.org/10.1016/j.jcat.2015.08.020>.

References

- [1] H.G. Manyar, B. Yang, H. Daly, H. Moor, S. McMonagle, Y. Tao, G.D. Yadav, A. Goguet, P. Hu, C. Hardacre, *ChemCatChem* 5 (2013) 506–512.
- [2] E. Bus, R. Prins, J.A. van Bokhoven, *Catal. Commun.* 8 (2007) 1397–1402.
- [3] B.-H. Zhao, J.-G. Chen, X. Liu, Z.-W. Liu, Z. Hao, J. Xiao, Z.-T. Liu, *Ind. Eng. Chem. Res.* 51 (2012) 11112–11121.
- [4] K. Taniya, H. Jinno, M. Kishida, Y. Ichihashi, S. Nishiyama, *J. Catal.* 288 (2012) 84–91.
- [5] X. Yang, D. Chen, S. Liao, H. Song, Y. Li, Z. Fu, Y. Su, *J. Catal.* 291 (2012) 36–43.
- [6] W. Lin, H. Cheng, L. He, Y. Yu, F. Zhao, *J. Catal.* 303 (2013) 110–116.
- [7] Q. Yu, X. Zhang, B. Li, J. Lu, G. Hu, A. Jia, C. Luo, Q. Hong, Y. Song, M. Luo, *J. Mol. Catal. A* 392 (2014) 89–96.
- [8] Y. Zhu, F. Zaera, *Catal. Sci. Technol.* 4 (2014) 955–962.
- [9] J. Serrano-Ruiz, A. López-Cudero, J. Solla-Gullón, A. Sepúlveda-Escribano, A. Aldaz, F. Rodríguez-Reinoso, *J. Catal.* 253 (2008) 159–166.
- [10] Z. Guo, C. Xiao, R.V. Maligal-Ganesh, L. Zhou, T.W. Goh, X. Li, D. Tesfagaber, A. Thiel, W. Huang, *ACS Catal.* 4 (2014) 1340–1348.
- [11] Z. Liu, X. Tan, J. Li, C. Lv, *New J. Chem.* 37 (2013) 1350–1357.
- [12] S. Bhogeswararao, D. Srinivas, *J. Catal.* 285 (2012) 31–40.
- [13] B.F. Machado, S. Morales-Torres, A.F. Pérez-Cadenas, F.J. Maldonado-Hódar, F. Carrasco-Marín, A.M. Silva, J.L. Figueiredo, J.L. Faria, *Appl. Catal. A* 425 (2012) 161–169.

- [14] Z. Sun, Z. Rong, Y. Wang, Y. Xia, W. Du, Y. Wang, *RSC Adv.* 4 (2014) 1874–1878.
- [15] L.J. Durndell, C.M. Parlett, N.S. Hondow, M.A. Isaacs, K. Wilson, A.F. Lee, *Sci. Rep.* 5 (2015) 9425–9433.
- [16] B. Coq, F. Figueras, *Coord. Chem. Rev.* 178 (1998) 1753–1783.
- [17] J. Zhao, M. Shao, D. Yan, S. Zhang, Z. Lu, Z. Li, X. Cao, B. Wang, M. Wei, D.G. Evans, *J. Mater. Chem. A* 1 (2013) 5840–5846.
- [18] X. Xiang, W. He, L. Xie, F. Li, *Catal. Sci. Technol.* 3 (2013) 2819–2827.
- [19] Y. Gao, Z. Zhang, J. Wu, X. Yi, A. Zheng, A. Umar, D. O'Hare, Q. Wang, *J. Mater. Chem. A* 1 (2013) 12782–12790.
- [20] P. Guerrero-Urbaneja, C. García-Sancho, R. Moreno-Tost, J. Mérida-Robles, J. Santamaría-González, A. Jiménez-López, P. Maireles-Torres, *Appl. Catal., A* 470 (2014) 199–207.
- [21] J. Feng, C. Ma, P.J. Miedziak, J.K. Edwards, G.L. Brett, D. Li, Y. Du, D.J. Morgan, G. J. Hutchings, *Dalton T.* 42 (2013) 14498–14508.
- [22] Z. Sun, L. Jin, S. He, Y. Zhao, M. Wei, D.G. Evans, X. Duan, *Green Chem.* 14 (2012) 1909–1916.
- [23] L. Chen, B. Sun, X. Wang, F. Qiao, S. Ai, J. Mater. Chem. B 1 (2013) 2268–2274.
- [24] K. Lee, D.A. Ruddy, G. Dukovic, N.R. Neale, *J. Mater. Chem. A* 3 (2015) 8115–8122.
- [25] K.S. Sing, *Pure Appl. Chem.* 57 (1985) 603–619.
- [26] K.S. Sing, R.T. Williams, *Adsorpt. Sci. Technol.* 22 (2004) 773–782.
- [27] P. Kluson, L. Cerveny, *Appl. Catal., A* 128 (1995) 13–31.
- [28] B. Wu, H. Huang, J. Yang, N. Zheng, G. Fu, *Angew. Chem.* 124 (2012) 3496–3499.